Application of near-ambient pressure X-ray photoelectron spectroscopy (NAP-XPS) in an in-situ analysis of the stability of the surface-supported metal-organic framework HKUST-1 in water, methanol and pyridine atmospheres

Marit Kjærvik [a], Paul M. Dietrich [b], Andreas Thissen [b], Jörg Radnik [a], Alexei Nefedov [c], Carsten Natzeck [c], Christof Wöll [c], Wolfgang E.S. Unger [a,*]

[a] *Bundesanstalt für Materialforschung und –prüfung, 12200, Berlin, Germany*
[b] *SPECS Surface Nano Analysis GmbH, Voltastraße 5, 13355, Berlin, Germany*
[c] *Institute of Functional Interfaces, Karlsruhe Institute of Technology (KIT), 76131, Karlsruhe, Germany*

ARTICLE INFO

Keywords:
Near-ambient pressure X-ray photoelectron spectroscopy
Metal-organic frameworks
HKUST-1
Interaction with atmospheres
Water
Methanol
Pyridine
Chemical state of copper

ABSTRACT

Surface-supported metal-organic frameworks HKUST-1 (Hong Kong University of Science and Technology) were used as a model system for a development of a near ambient pressure (NAP) XPS based approach to investigate interaction with atmospheres of water, methanol or pyridine at pressures ranging from 1 to 4 mbar. The films were grown on a gold substrate functionalized with a COOH-terminated self-assembled monolayer using liquid-phase epitaxy in a step-by-step fashion. Measurement protocols were developed and optimised for different gases in order to obtain spectra of similar quality in terms of signal intensity, noise and shape. Peak shapes were found to depend on the efficiency of charge compensation. Reference measurements in argon proved to be a useful strategy not only for the evaluation of the Cu(II)-fraction in pristine samples, but also to identify the contributions by the respective gas atmosphere to the C 1s and O 1s photoelectron spectra. Reduced copper was found during the exposition of HKUST-1 to water vapour and pyridine, but this effect was not observed in case of methanol. Additionally, it was established that there are no changes in relative Cu(II) percentage with increasing exposure time. This indicates that saturation was reached already at the lowest time of gas exposure. A detailed elucidation of the mechanism of Cu(II) reduction to Cu(I) in HKUST-1 mediated by water and pyridine is part of ongoing work and not in the scope of the present paper.

1. Introduction

Metal–organic frameworks (MOFs) are constructed from coordinated metal ions or metal-oxo clusters, acting as nodes, and organic building blocks, referred to as linkers [1]. More than 70.000 MOFs have been synthesized so far [2], and the number of MOFs which have an associated theoretical description is roughly one million. Originally developed for such applications as gas storage [3], gas separation [4–7] and catalysis [8,9], in recent years it has been shown that these porous, crystalline solids also have enormous potential in completely different areas. For many advanced applications in nanotechnology, it is necessary that the MOFs, usually obtained in powder form, are deposited on solid substrates. These so called surface-supported metal–organic frameworks (SURMOFs) [10], fabricated using layer-by-layer methods, are receiving increasing attention as a novel form of nanotechnology [11,12]. Recently developed deposition techniques enable control of film thickness, homogeneity, morphology and dimensions for a huge number of MOF compounds, which offers tremendous opportunities in different application fields, such as energy storage, water splitting, CO_2 reduction, as well as for the fabrication of membranes. These applications meet the increasing demands for environmental sustainability and cleaner energy.

The metal–organic framework HKUST-1 (Hong Kong University of Science and Technology) was introduced by Williams et al. [13] and is also known as CPO-27 and $Cu_3(BTC)_2$. It consists of Cu(II)-dimers linked together with 1,3,5-benzenetricarboxylate (BTC), forming a highly

* Corresponding author.
E-mail address: wolfgang.unger@alumni.hu-berlin.de (W.E.S. Unger).

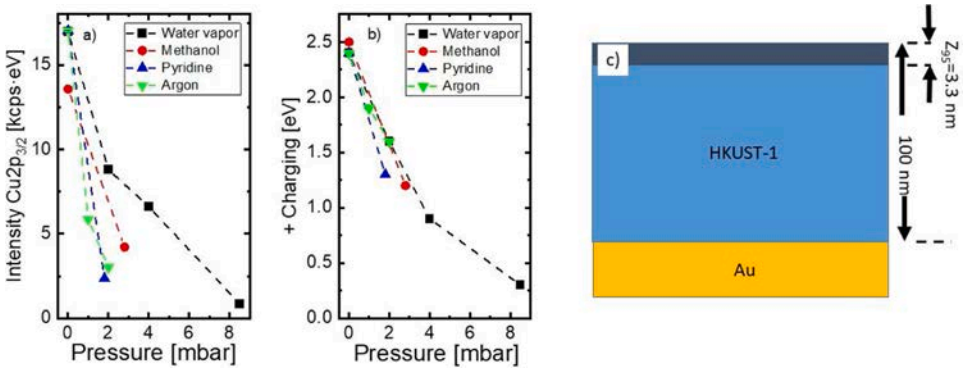

Fig. 1. Cu $2p_{3/2}$ intensity expressed as area under the spectrum (a) and charging relative to the aliphatic carbon component binding energy set to 285.0 eV (b) for the respective atmospheres at pressures ranging from 10^{-5} mbar to 8 mbar. Scheme of the analysed SURFMOF HKUST-1/Au sample showing its total thickness and the information depth z_{95} of Cu 2p photoelectrons (c), as defined by term 4.245, Note 2, ISO 18115-1(2013) [30].

crystalline 3D-network, which has shown very promising performance for both gas storage and separation techniques, and activity for diverse Lewis-acid catalysed reactions [14].

Although existing applications are encouraging, SURMOF thin films still face numerous challenges, including the need for a more thorough understanding of the stability of the internal and external interfaces, especially in a presence of different gases and water vapour. In particular, a known concern about HKUST-1 and other MOFs is their instability under humidity, which limits their use in ambient working conditions [15]. X-ray diffraction (XRD) has shown that the crystal structure of HKUST-1 is still intact after exposure to water vapour, although the uptake of gases is dramatically decreased. This indicates that so called surface barriers are responsible for the behaviour observed [16].

With that in mind, near-ambient pressure X-ray photoelectron spectroscopy (NAP-XPS) is a unique method for in-situ investigations of SURMOFs under gas/vapour exposure. With recent instrumental advances, samples can routinely be characterised in the mbar-range, allowing the answering of important questions about the sample's stability and interaction with gas molecules. HKUST-1 is an extensively studied SURMOF system and is therefore a suitable model system for developing NAP-XPS measurement protocols for MOFs. Analysis of Cu 2p-photoelectron and Cu *LMM* Auger spectra allows to determine the relative amount of Cu(I) and Cu(II)-species, giving significant information on the pristine state and the stability of HKUST-1 s under near-ambient pressure conditions.

Previous XPS studies show that HKUST-1 samples contain Cu(I)-species [17–20], with relative amounts of Cu(I) and Cu(II) changing with heating, X-ray irradiation or exposure to such gases as H_2, O_2, NO, CO or water vapour [18,20–23]. NAP-XPS studies of the effect of different gases on HKUST-1 have previously been reported by Nijem et al., exposing the samples for up to 0.03 mbar NH_3 [19] and 0.27 mbar NO [24]. Both studies also included loading the samples with water vapour, in order to study an adsorption of gas molecules at both dry and humid conditions. In the first study [19] the authors found that ammonia replaces water at unsaturated Cu(II)-centres, while the second [24] showed an enhanced adsorption of nitric oxide with an increase in the number of Cu(I)-sites following thermal treatment or X-ray irradiation.

Since Cu(II)-species are sensitive to X-ray irradiation and even pristine samples can be assumed to contain Cu(I) ions, the experimental strategy and the interpretation of NAP-XPS results should be carefully considered. In this paper, we analyse SURMOF HKUST-1 in NAP-XPS investigations under water-, methanol- and pyridine atmospheres at pressures ranging from 1 to 4 mbar. Measurement conditions were optimised for different atmospheres to obtain spectra of similar quality in terms of signal intensity, noise and shape where the latter one is determined by the efficiency of charge compensation. Reference measurements under argon proved to be a useful strategy not only for the evaluation of Cu(II)-fractions in pristine samples, but also of C 1s and O 1s XP spectra. Since the photoelectron signal of gas phase water, methanol and pyridine partly overlaps with the C 1s and O1s photoelectron signal from HKUST-1, comparison with reference spectra acquired under argon atmosphere is helpful for peak fitting analysis.

2. Experimental

2.1. Sample preparation

All HKUST-1 SURMOFs were grown on the gold surface functionalized with a COOH-terminated self-assembled monolayer (SAM) to promote the formation of preferentially oriented films in [100] direction with a high degree of structural perfection [25,26]. To grow SAM layers, silicon substrates coated with a 150 nm thick gold film with a roughness of 2–3 nm were immersed into ethanolic solutions of 16-mercaptohexadecanoic acid for 72 h. The SURMOF synthesis was performed as liquid-phase epitaxy (LPE) in a step-by-step fashion, in which the functionalized substrate is sequentially and repeatedly exposed to an ethanolic metal salt solution and an ethanolic linker solution. Between each step the surface is cleaned with pure ethanol. For HKUST-1 SURMOFs, ethanolic solutions of Cu(II) acetate (1 mM $Cu(OAc)_2$) and ethanolic 1,3,5-benzenetricarboxylic acid (0.2 mM H_3BTC) were used. Recently, reasonable progress in the procedure of the HKUST-1 growth was achieved. Thus, firstly, it was established that the water content in the synthesis solutions has a tremendous impact on the crystallinity of the HKUST-1 films. In this study we used 10 vol % water in the linker solution to get high crystallinity in films as recently recommended by Müller et al. [27]. Secondly, it was found that an additional ultrasonication during the immersion of the sample in pure ethanol results in a decrease of the defect density in high-quality (HQ)-HKUST-1 SURMOF films. In such HQ-HKUST-1 films the amount of Cu(I) sites is usually less 4% [20]. The HKUST-1 films were prepared in a nitrogen filled glove box automatically regulated humidity (here 9–11 %) and an automated six-axis robot TX 60 from Staubli (Pfaffikon, Switzerland) with a pneumatic gripper system, for further details see Z. G. Gu et al. [28]. The functionalized substrate was dipped successively in metal salt solution, pure ethanol, linker solution and again pure ethanol for 10 min, 1 min, 15 min, 1 min, respectively. Between each step, the sample was rinsed with pure ethanol for 5 s. The desired thickness can be adjusted using a number of distinct LPE cycles. In this study, 40 cycles were used, which resulted in a total film thickness of approximately 100 nm, as illustrated in Fig. 1c. After the epitaxial growth of the SURMOFs, samples were characterized by X-ray diffraction (XRD) using a D8-Advance Bruker AXS diffractometer (Cu Kα-radiation, λ 1.5418 Å) in $\theta/2\theta$ geometry. The obtained XRD data are presented in Fig. SI1 in the Supplementary Information (SI).

2.2. NAP-XPS measurements

Measurements were performed with an EnviroESCA, a laboratory NAP-XPS instrument manufactured by SPECS Surface Nano Analysis GmbH (Berlin, Germany). The instrument is equipped with a monochromatic Al K_α X-ray source, which is separated from the sample environment by a silicon nitride window. The first aperture towards the spectrometer is 300 μm in diameter, and the working distance is approximately the same. It is followed by a three-stage differential pumping system for a rapid pressure drop to 10^{-9} mbar before the photoelectrons enter the hemispherical energy analyser held at UHV conditions. For more instrumental details, see P.M. Dietrich et al. [29]. For gas exposure, a glass vial filled with the respective degassed liquid was connected to the chamber by a leak valve. In these experiments, argon (99.999 %, Air Liquide), water (ultrapure HPLC grade, Alfa Aesar), methanol (99.9 %, Merck) and pyridine (99.8 %, Sigma Aldrich) were used.

In NAP-conditions, the signal attenuation due to scattering of photoelectrons by gas molecules must be considered. Due to different scattering cross sections, the attenuation varies among different kinds of gases. Fig. 1a shows how the intensity of the Cu $2p_{3/2}$ peak decreases with increasing pressure for water vapour, methanol, pyridine and argon.

The combination of a gas atmosphere, especially argon, and an electron flood gun is known as dual mode charge compensation [31]. An electron flood gun is not compatible with NAP-conditions due to the hot filament emitter. However, the environment of ionized gas and free electrons in NAP-XPS provides effective charge compensation for non-conducting samples [29]. The charge compensation and stabilization in the different atmospheres is illustrated in Fig. 1b by displaying the charging relative to the C 1s core level peak of aliphatic (adventitious) carbon at 285.0 eV. It is necessary to mention that the use of low energy electrons from a flood gun can cause reduction of Cu, as shown e.g., for NOTT-100 MOFs by Edwards et al. [31].

With the goal of obtaining photoelectron spectra with a comparable quality in different gas atmospheres, the pressure was chosen such that the measured absolute Cu $2p_{3/2}$ intensity was always in the same range, while the pressure was high enough for sufficient charge compensation, i.e., 1 mbar for argon, 2 mbar for pyridine, 3 mbar for methanol and 4 mbar for water vapour. The motivation for reference measurements at 1 mbar of argon was to use argon as an inert atmosphere for effective charge compensation, stabilization of the surface charge and to get reference spectra of the as received HKUST-1 sample with similar full width at half maximum (FWHM) as for those measured under reactive atmospheres. Additionally, it is an advantage that the core level photoemission lines of argon do not overlap with that of any other elements of interest.

X-ray induced degradation of Cu(II)-species is common for Cu(II)-species in general [32–34] and has also been observed for HKUST-1 before [22,24]. This behaviour was clearly observed during our measurements as well (see Fig. SI2a and SI5 in SI). By a careful design of the measurement protocol, we minimized the effect of beam induced damage for the data presented in the main paper. This was done by reducing the acquisition time for the Cu $2p_{3/2}$ spectra to 7 min, and the Cu LMM Auger spectra to 5 min, which was found to be the shortest acquisition time possible while obtaining spectra of meaningful quality. Further, the measurement spot was changed for each new set of measurements. We always used the following order of acquisition: Cu $2p_{3/2}$, Cu LMM, C 1s, O 1s, survey. All core level spectra were acquired at 30 eV pass energy, 0.25 s dwell time and 0.1 eV energy step width. Survey spectra were acquired at 100 eV pass energy, 0.1 s dwell time and 1 eV energy step width.

2.3. Data analysis

UNIFIT 2018 was used for XPS peak analysis [35]. The two satellite peaks of the Cu(II)-species were fitted with a Gaussian shape, and the Cu (II) main component peak was generally fitted using a higher FWHM and a somewhat larger Lorentzian contribution than in the case of the Cu(I) component peak as recommended in the literature [32]. Since the FWHM decreases at increasing pressures due to the environmental charge compensation under NAP conditions [29], the FWHM was different for each measurement condition. The Lorentzian-Gaussian mixing factor was kept constant at 0.2 for Cu(I) and 0.3 for Cu(II), values which were found to be the most appropriate by trial and error during peak fit analysis. Furthermore, the binding energy of Cu(I) and Cu(II) component peaks were constrained to 933.2 ± 0.1 eV and 935 ± 0.1 eV, which is in good agreement with other XPS studies of HKUST-1 [20,22]. The relative amounts of Cu(I) and Cu(II) was calculated directly from the relative areas of the peak components obtained from peak fitting. The distinction between Cu(I) and Cu(II) species is discussed in detail in Chapter SI2, of the Supporting Information. The parameters used for peak analysis are listed in Table 1. The binding energy scale was corrected for static charging with respect to the C 1s component peak of aliphatic (adventitious) carbon at 285.0 eV, in accordance with ISO 19318:2004 [36]. The background was fitted in parallel with the peak fit, with a Shirley background for O 1s and C 1s spectra, and for the Cu $2p_{3/2}$ spectra with a Tougaard background. For graphical representation, the XP spectra were normalised to maximum intensity.

The error in peak intensities from the peak fit for Cu(II) was estimated by matrix inversion as offered by the UNIFIT software [35]. The calculated errors for peak components are listed in Table SI2, SI.

Table 1
Overview of parameters used for peak analysis by UNIFIT 2018 software [35]. LG = 0 defines a pure Gaussian peak shape function and LG = 1 a pure Lorentzian function. (g) identifies gas phase measurements.

XP-spectrum	Component	Binding energy [eV]	LG-mixing ratio
Cu $2p_{3/2}$	Cu(I)	933.2 ± 0.1	0.2
	Cu(II)	935.1 ± 0.1	0.3
	Satellite 1	940.3 ± 0.3	0
	Satellite 2	944.5 ± 0.3	0
C 1s	C—C, C—H	285.0	0.1
	C—O	286.4 ± 0.1	0.1
	O═C—O	288.8 ± 0.2	0.1
	Methanol (g)	288.0	0
	Pyridine (g)	286.5	0.2
O 1s	O═C—O	532.0	0.1
	H_2O_{ads} + other CHO contamination species	533.3 ± 0.2	0.1
	Methanol (g)	534.5	0.2
	Water vapour	535.4	0.2

3. Results and discussion

The Cu $2p_{3/2}$, C 1s and O1s XP spectra and the Cu *LMM* Auger spectrum were measured first in 1 mbar argon as reference (Fig. 2) for all the other results acquired in water, methanol and pyridine atmospheres. The Cu $2p_{3/2}$ XP spectrum (Fig. 2a) shows a main peak at a binding energy of 935.1 eV assigned to Cu(II)-species, and two distinct satellite peaks at binding energies of 944.2 eV and 940.0 eV, which are exclusively associated with Cu(II)-species. A minor peak at 933.2 eV is assigned to emerging Cu(I)-species, contributing approximately 2 % of the total Cu atomic fraction. This number is in accordance with previous XPS investigations of HKUST-1 samples in ultra-high vacuum, which report Cu(I) fractions of 3–6 % [17,18,20] in pristine samples.

The C 1s XP spectrum is presented in Fig. 2c and it can be fitted with three components, one at 285.0 eV originating from the aromatic ring in BTC, one at 286.4 eV assigned to C—O species and one at 288.8 eV from the carboxylic groups in BTC. The O 1s XP spectrum is shown in Fig. 2d. It is known that in the HKUST-1 structure, each Cu-atom is bound to 5

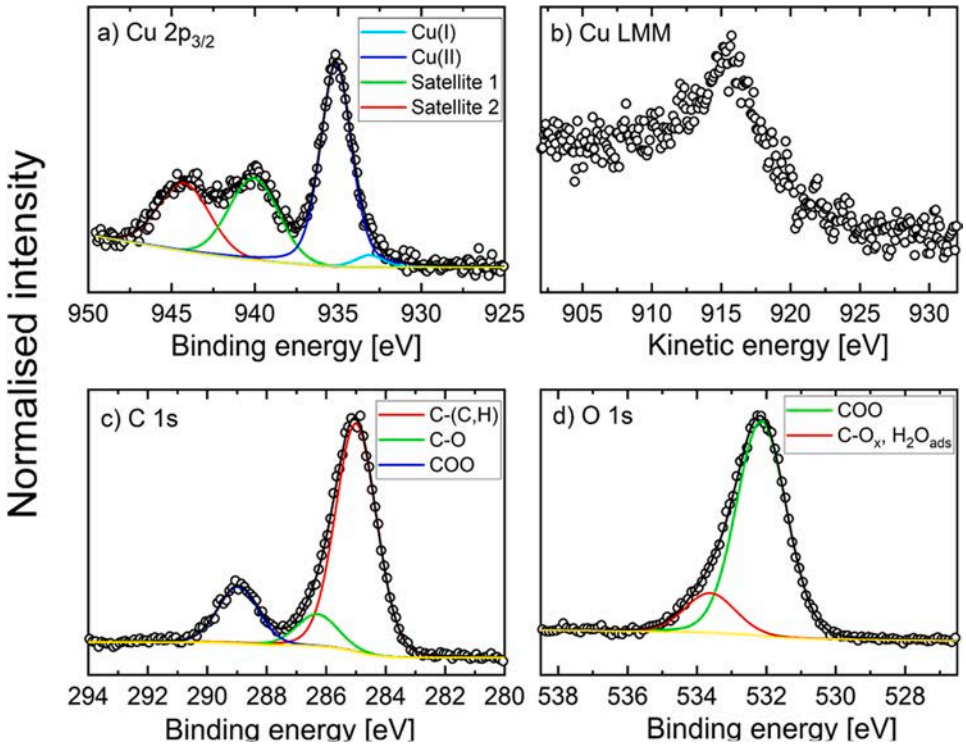

Fig. 2. The Cu $2p_{3/2}$ (a), C 1s (c) and O 1s (d) XP spectra and Cu LMM Auger spectrum (b) of HKUST-1 acquired in 1 mbar argon atmosphere characterizing the pristine state of sample.

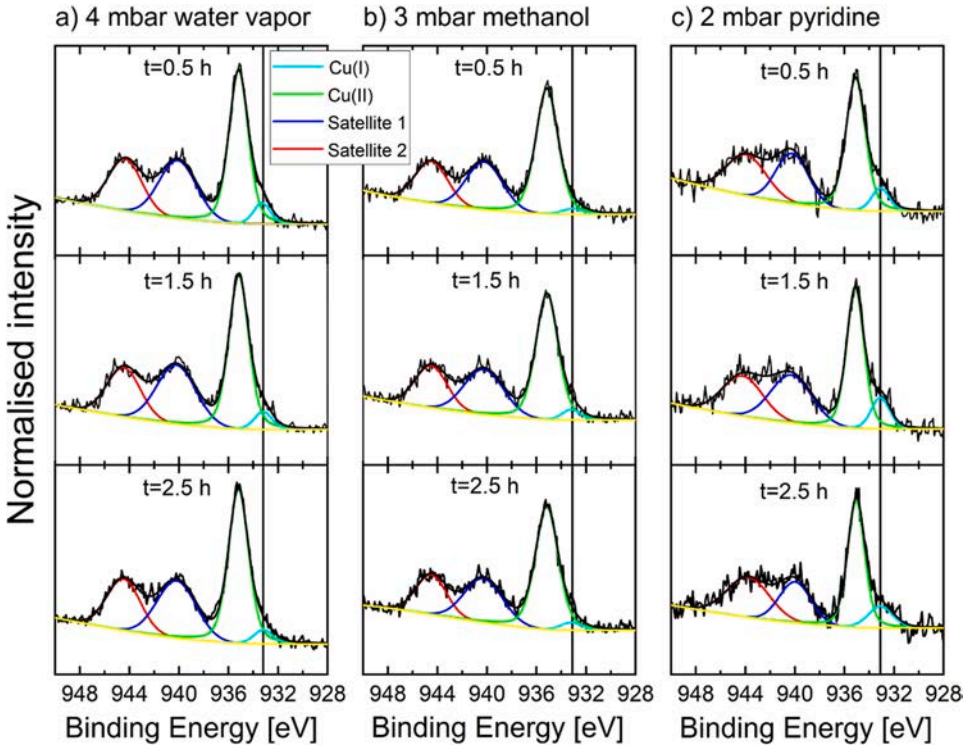

Fig. 3. The Cu $2p_{3/2}$ XP spectra of HKUST-1 exposed to 4 mbar water vapour (a), 3 mbar methanol (b) and 2 mbar pyridine (c), after 0.5 h, 1.5 h and 2.5 h of exposure. The vertical line indicates the contribution from Cu(I) at binding energy 933.2 eV.

oxygen atoms, 4 of them as part of the BTC-linker and one from adsorbed water. Thus, the broad main component at 532.0 eV of the O 1s spectrum (Fig. 2d) is assigned to carboxyl group oxygen atoms from the BTC-linker. This broad peak covers the photoemission originating from both carboxylic oxygen species. In addition, a feature at higher binding energy is observed at ~533.3 eV and may be assigned to a superposition of contributions of adsorbed water and other species from CHO contaminants as discussed by Trotochaud et al. [37].

Table 2
Overview of the relative Cu(I)-fraction at the various pressures and exposure times.

Gas	Pressure	Exposure time (h)	Exposure (10^8 L[a])	% Cu(I)
Argon	1 mbar	0.5	1.4	2
		0.5	5.4	5
		1.5	16.2	4
Water vapour	4 mbar	2.5	27	4
		3.5	37.8	4
		4.5	48.6	4
		16.5	178	6
		0.5	3.7	1
		1.5	10.9	3
Methanol	3 mbar	2.5	18.2	3
		3.5	25.5	3
		4.5	32.8	3
		0.5	2.4	7
Pyridine	2 mbar[b]	1.5	7.3	9
		2.5	13.8	9

[a] 1 Langmuir [L] equals to the gas exposure of 10^{-6} Torr for 1 s.
[b] The pressure was increased to maximum 5 mbar after 2 h exposure.

Then we started to study the stability of HKUST-1 SURMOFs in the presence of reactive atmospheres. Fig. 3 displays the fitted Cu $2p_{3/2}$ NAP-XP spectra of HKUST-1 exposed to 4 mbar water vapour (a), 3 mbar methanol (b) and 2 mbar pyridine (c) atmospheres after 0.5 h, 1.5 h and 2.5 h exposure. The vertical line at 933.2 eV indicates the position of Cu(I)-species. The complete dataset of the relative Cu(I)-fraction at the various pressure conditions and exposure times is listed in Table 2. Minor variations in the amount of Cu(II) relative to that of reduced Cu-species have been found, however, they are dependent on type of absorbed molecules from the different atmospheres. Within the error of the peak fit analysis (see Table SI2 in SI), there are no changes in relative Cu(II) percentage with increasing exposure time pointing to saturation reached in the analysed surface layer (cf. Fig. 1c) already at the lowest time of exposure. This result confirms previous observations for ammonia in HKUST-1 [22], where the saturation effect was found at very low exposures as well.

The result is that the Cu(I) contribution is negligible for samples exposed to argon and methanol, but it is approximately 4% for samples exposed to water vapour and 8 % for samples exposed to pyridine. A similar value, ~6 %, was obtained by Nijem et al. for HKUST-1 exposed to 0.01 Torr water or 0.26 Torr NH_3 [19]. Despite much higher exposures in our case, we assume that the adsorption mechanism for water molecules should be the same as proposed by Nijem et al. It is important to mention that, despite small changes of electronic configuration of copper metallic centres as concluded from XPS, the HKUST-1 structure, as it was confirmed with XRD measurements (see Fig. SI1 in SI), remains stable.

A subsequent step of the project, the elucidation of the mechanism of Cu(II) reduction to Cu(I) in HKUST-1 mediated by water and pyridine is part of ongoing work. So far the mechanism of the Cu(II) reduction remains unclear. A collaboration with a theory group was launched to identify possible mechanisms. In case of exposure of H-KUST-1 to water dissociation/deprotonation might be one of possible routes.

The Cu *LMM* Auger spectra acquired under the various atmospheres are presented in Fig. SI3, SI. Moreover, the Wagner plot, displaying the Cu $2p_{3/2}$ binding energy versus the kinetic energy of the maximum intensity in the Cu *LMM* Auger spectrum is shown in Fig. SI4, SI. Such data presentation is a useful tool for characterising the copper species, especially when it is necessary to compare experimental results with reference data. The corresponding data are summarized in Table SI1, SI. The Wagner plot in Fig. SI4 confirms the XPS results. The figure shows that the data points from Cu $2p_{3/2}$ in water vapor, methanol and pyridine are close to the one from argon, meaning that there are only minor differences in electronic configuration under the different conditions.

The copper dimers in HKUST-1 are linked by 1,3,5-benzenetricarboxylate units (BTC^{2-}), the chemical structure of which is displayed in Fig. 4d. Thus, not only the Cu 2p XP spectra but also the C 1s and O 1s XP spectra can provide useful information on the stability of HKUST-1 under gas exposure. However, in NAP-XPS the gas phase peak may overlap with photoelectron signals from the sample, which is the case for the C 1s spectra for the experiments using exposure to methanol or pyridine, and the O 1s spectra for the experiments under exposure to methanol or water vapour. This superposition complicates peak fitting analysis and interpretation of the spectra. Two approaches for distinguishing the photoelectron signals from the gas/vapour itself and HKUST-1 in the C 1s and O1s XP spectra are proposed. The simplest approach is to superpose the spectra with reference spectra acquired in argon atmosphere, as shown in the upper row of Fig. 4b, c for C 1s and Fig. 5a, b for O 1s XP spectra. This approach is appropriate for qualitative analysis only, however, the information obtained from it is helpful for the spectra quantification using a peak fitting procedure. Here an evaluation of difference spectra as displayed Fig. 6 helps to identify the O 1s or C 1s binding energies of the respective component peaks in the

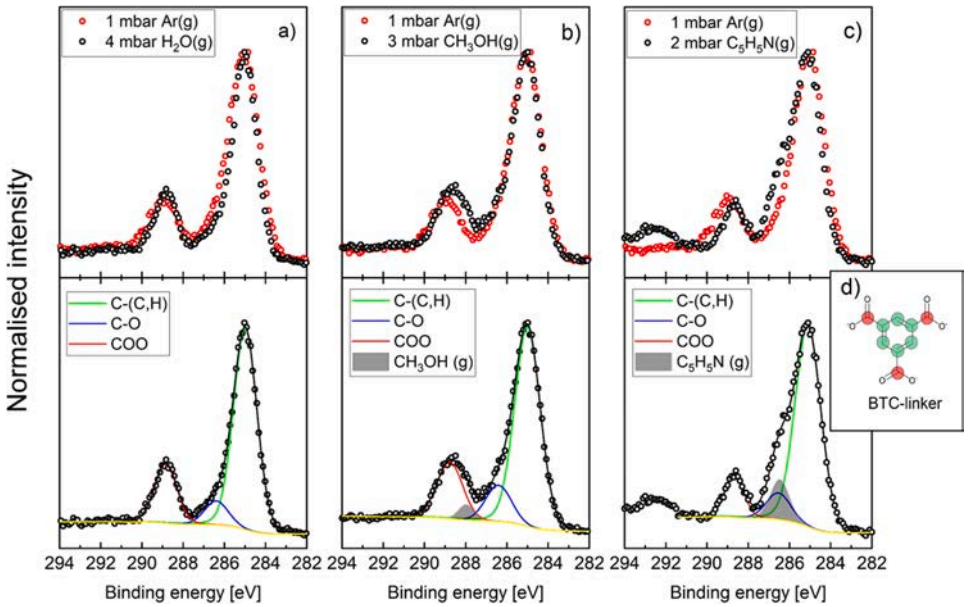

Fig. 4. The C1s NAP-XP spectra of HKUST-1 exposed to water vapour (a), methanol (b) and pyridine (c) atmospheres after 0.5 h exposure. The upper set of spectra compares the C1s spectra under NAP-XPS conditions with reference measurements of HKUST-1 in 1 mbar argon, while the lower spectra show the peak fitting analysis of the NAP-XP spectra. Component peaks originating from the environment atmosphere are shown in grey. The chemical structure of the organic linker BTC^{2-} is shown in d), highlighting the two types of carbon bonds found in the linker: aromatic carbon (green) and carboxylic carbon (red).

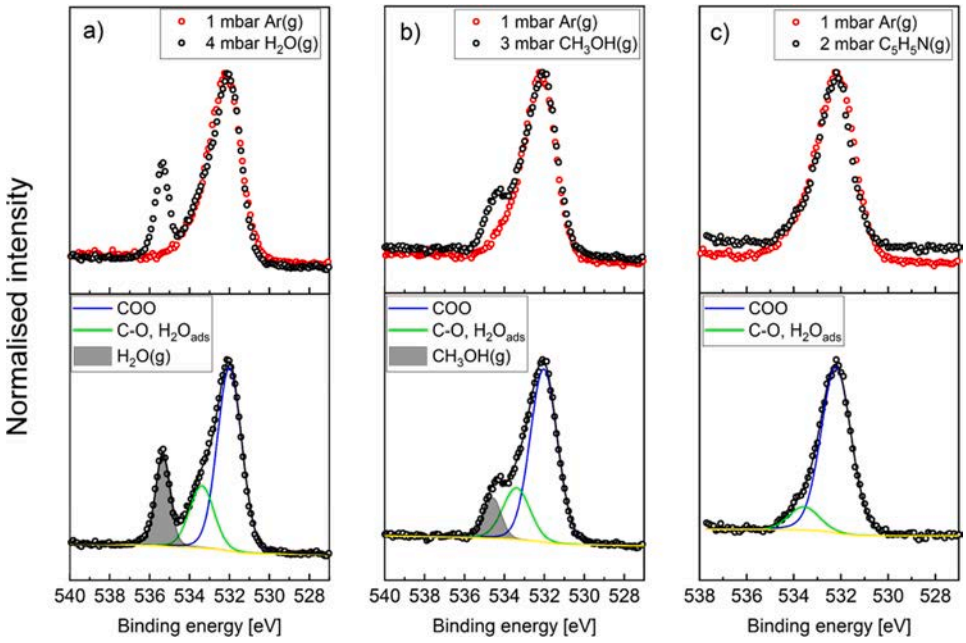

Fig. 5. The O1s NAP-XP spectra of HKUST-1 exposed to water vapour (a), methanol (b) and pyridine (c) after 0.5 h exposure. The upper set of spectra compares the O1s peak under NAP-XPS conditions with reference measurements of HKUST-1 in 1 mbar argon, while the lower spectra show the fitted peaks of the NAP-XP spectra. Components originating from the environment atmosphere are shown in grey.

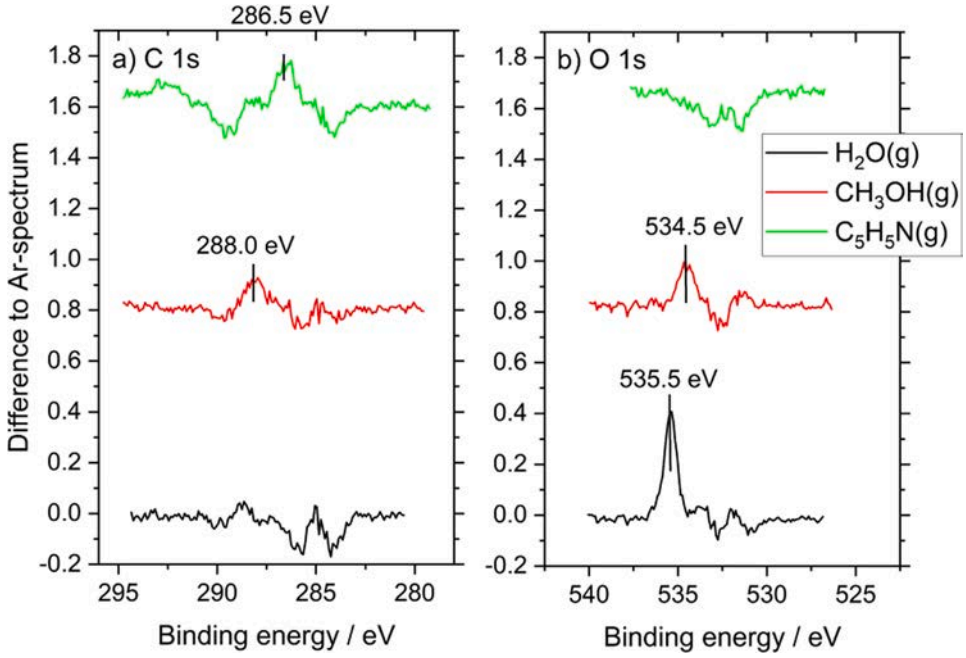

Fig. 6. Difference spectra obtained by using normalized O 1s and C 1s NAP-XP spectra of HKUST-1 exposed to water vapour, methanol or pyridine after 0.5 h exposure and the respective spectra acquired under Ar atmosphere. The resulting O 1s and C 1s binding energies of the component peaks related to the different gaseous species are given by numbers. Note that the spectra of HKUST-1 exposed to methanol or pyridine are shifted upwards by 0.8 and 1.6 units, respectively.

spectra resulting from gaseous species. Finally, Fig SI7 shows that C1s and O1s spectra do not change vs. increasing exposure-time. This was proved for 0.5 h and 4.5 h exposure to 4 mbar water and 3 mbar methanol.

In the second approach an attempt to fit the gas phase peak is done. The XPS signals from the respective gas/vapour phase can be distinguished accurately from the sample signal by peak fitting analysis and is shown in the lower row of Figs. 4 and 5. Peak fitting is straight forward for the water vapour O 1s core level peak in Fig. 5a, which is well separated in binding energy. However, it is more challenging for the C1s peak acquired in methanol and pyridine atmosphere (Fig. 4b, c), where the gas phase peak is less distinct. As already mentioned, the evaluation of difference spectra (cf. Fig. 6) helps to identify binding energies of the respective component peaks resulting from gaseous species. As input to the peak fit analysis, the XP spectra of the pure gas phase at each condition have also been measured, these are displayed in Fig. SI6. Details on the peak fitting parameters are presented in Table 1.

No obvious changes were observed for the second O1s component at

533.3 eV after the exposure to water vapour in comparison with measurements in argon atmosphere. We therefore cannot confirm water dissociation as concluded from the IR-data reported by Safy et al. [16]. For OH^- species attached to Cu(II) we would expect a O1s position of 532.9 ± 0.3 eV, (typical values for M-OH species [38]). Unfortunately, this binding energy overlaps with the photoemission peak at 533.3 eV measured with the pristine sample in Argon armosphere. As a result, the present O 1s data do not allow to judge on the presence or absence of OH species bound to the HKUST-I metal centers.

4. Conclusion

In this paper, it was demonstrated that our NAP-XPS approach to study gas adsorption on SURMOFs using HKUST-1 as a model in a development of a near ambient pressure (NAP) XPS based protocol to investigate interaction with reactive gas atmospheres at pressures up to a few mbar was successful. In this study HKUST-1 SURMOF films were grown on a gold surface functionalized with a COOH-terminated SAMs using LPE in a step-by-step fashion. NAP-XPS measurement protocols were optimised to obtain spectra acquired under exposure to the different gases at comparable quality in terms of signal intensity, noise and peak shape, the latter affected by charge compensation by the ionized gas atmosphere to which the SURMOF film was exposed. The upper pressure limit at which we can obtain useful information from the Cu $2p_{3/2}$ core level spectra was determined to be 4 mbar for water vapor, 3 mbar for methanol and 2 mbar for pyridine. Reference NAP-XPS measurements in argon atmosphere proved to be a useful strategy not only for the evaluation of Cu(II) fraction in pristine samples, but also for separation of the photoelectron signals originating from HKUST-1 and the respective gas atmosphere in the C 1s and O 1s XP spectra. Additionally, compared to the reference spectrum, a reduced copper species was found during the exposure to water vapour and pyridine, but was not observed in case of exposure to methanol. It was also established that there were no changes in the relative fraction Cu(II) species with increasing exposure time, indicating that saturation is reached already at the lowest time of exposure which was 30 min in this study. The analysis of the C 1s and O 1s spectra showed the stability of the organic linker in the SURMOF film under the chosen conditions.

Acknowledgements

Financial support from BAM and the Helmholtz Association is gratefully acknowledged. Furthermore, we thank Nina Scheuermann, Institute of Functional Interfaces of KIT, for the excellent support during preparation of the HKUST-1 samples.

References

[1] O.M. Yaghi, Reticular chemistry—Construction, properties, and precision reactions of frameworks, J. Am. Chem. Soc. 138 (2016) 15507–15509, https://doi.org/10.1021/jacs.6b11821.
[2] P.Z. Moghadam, A. Li, S.B. Wiggin, A. Tao, A.G.P. Maloney, P.A. Wood, S.C. Ward, D. Fairen-Jimenez, Development of a Cambridge structural database subset: a collection of metal–organic frameworks for past, present, and future, Chem. Mater. 29 (2017) 2618–2625, https://doi.org/10.1021/acs.chemmater.7b00441.
[3] M. Eddaoudi, J. Kim, N. Rosi, D. Vodak, J. Wachter, M. O'Keeffe, O.M. Yaghi, Systematic design of pore size and functionality in isoreticular MOFs and their application in methane storage, Science 295 (2002) 469–472, https://doi.org/10.1126/science.1067208.
[4] A.J. Brown, N.A. Brunelli, K. Eum, F. Rashidi, J.R. Johnson, W.J. Koros, C. W. Jones, S. Nair, Interfacial microfluidic processing of metal-organic framework hollow fiber membranes, Science 345 (2014) 72–75, https://doi.org/10.1126/science.1251181.
[5] Y. Peng, Y. Li, Y. Ban, H. Jin, W. Jiao, X. Liu, W. Yang, Metal-organic framework nanosheets as building blocks for molecular sieving membranes, Science 346 (2014) 1356–1359, https://doi.org/10.1126/science.1254227.
[6] T. Rodenas, I. Luz, G. Prieto, B. Seoane, H. Miro, A. Corma, F. Kapteijn, F.X. Llabrés i Xamena, J. Gascon, Metal–organic framework nanosheets in polymer composite materials for gas separation, Nat. Mater. 14 (2015) 48–55, https://doi.org/10.1038/nmat4113.
[7] Z. Wang, A. Knebel, S. Grosjean, D. Wagner, S. Brase, C. Woll, J. Caro, L. Heinke, Tunable molecular separation by nanoporous membranes, Nat. Commun. 7 (2016), 13872, https://doi.org/10.1038/ncomms13872.
[8] H. Furukawa, K.E. Cordova, M. O'Keeffe, O.M. Yaghi, The chemistry and applications of metal-organic frameworks, Science 341 (2013), 1230444, https://doi.org/10.1126/science.1230444.
[9] T. Zhang, W. Lin, Metal–organic frameworks for artificial photosynthesis and photocatalysis, Chem. Soc. Rev. 43 (2014) 5982–5993, https://doi.org/10.1039/C4CS00103F.
[10] J. Liu, C. Woll, Surface-supported metal–organic framework thin films: fabrication methods, applications, and challenges, Chem. Soc. Rev. 46 (2017) 5730–5770, https://doi.org/10.1039/C7CS00315C.
[11] D. Zacher, O. Shekhah, C. Woll, R.A. Fischer, Thin films of metal–organic frameworks, Chem. Soc. Rev. 38 (2009) 1418–1429, https://doi.org/10.1039/b805038b.
[12] O. Shekhah, J. Liu, R.A. Fischer, C. Woll, MOF thin films: existing and future applications, Chem. Soc. Rev. 40 (2011) 1081–1106, https://doi.org/10.1039/c0cs00147c.
[13] S.S.Y. Chui, S.M.F. Lo, J.P.H. Charmant, A.G. Orpen, I.D. Williams, A chemically functionalizable nanoporous material $[Cu_3(TMA)_2\ (H2O)_3]_n$, Science 283 (1999) 1148–1150, https://doi.org/10.1126/science.283.5405.1148.
[14] T. Granato, F. Testa, R. Olivo, Catalytic activity of HKUST-1 coated on ceramic foam, Microporous Mesoporous Mater. 153 (2012) 236–246, https://doi.org/10.1016/j.micromeso.2011.12.055.
[15] M.E.A. Safy, M. Amin, R.R. Haikal, B. Elshazly, J. Wang, Y. Wang, C. Woll, M. H. Alkordi, Probing the water stability limits and degradation pathways of metal-organic frameworks (MOFs), Chem. – A Eur. J. (2020), https://doi.org/10.1002/chem.202000207 chem.202000207.
[16] L. Heinke, Z. Gu, C. Woll, The surface barrier phenomenon at the loading of metal-organic frameworks, Nat. Commun. 5 (2014) 4562, https://doi.org/10.1038/ncomms5562.
[17] P.St. Petkov, G.N. Vayssilov, J. Liu, O. Shekhah, Y. Wang, C. Woll, T. Heine, Defects in MOFs: a thorough characterization, ChemPhysChem 13 (2012) 2025–2029, https://doi.org/10.1002/cphc.201200222.
[18] K. Müller, N. Vankova, L. Schottner, T. Heine, L. Heinke, Dissolving uptake-hindering surface defects in metal-organic frameworks, Chem. Sci. 10 (2019) 153–160, https://doi.org/10.1039/c8sc03735c.
[19] N. Nijem, K. Fürsich, H. Bluhm, S.R. Leone, M.K. Gilles, Ammonia adsorption and co-adsorption with water in HKUST-1: spectroscopic evidence for cooperative interactions, J. Phys. Chem. C 119 (2015) 24781–24788, https://doi.org/10.1021/acs.jpcc.5b05716.
[20] W. Wang, D.I. Sharapa, A. Chandresh, A. Nefedov, S. Heißler, L. Heinke, F. Studt, Y. Wang, C. Woll, Interplay of electronic and steric effects to yield low-temperature CO oxidation at metal single sites in defect-engineered HKUST-1, Angew. Chemie Int. Ed. (2020), https://doi.org/10.1002/anie.202000385.
[21] J. Szanyi, M. Daturi, G. Clet, D.R. Baer, C.H.F. Peden, Well-studied Cu–BTC still serves surprises: evidence for facile Cu2+/Cu+ interchange, Phys. Chem. Chem. Phys. 14 (2012) 4383, https://doi.org/10.1039/c2cp23708c.
[22] A.S. Duke, E.A. Dolgopolova, R.P. Galhenage, S.C. Ammal, A. Heyden, M.D. Smith, D.A. Chen, N.B. Shustova, Active sites in copper-based metal–organic frameworks: understanding substrate dynamics, redox processes, and valence-band structure, J. Phys. Chem. C 119 (2015) 27457–27466, https://doi.org/10.1021/acs.jpcc.5b08053.
[23] S. Poulston, P.M. Parlett, P. Stone, M. Bowker, Surface oxidation and reduction of CuO and Cu2O studied using XPS and XAES, Surf. Interface Anal. 24 (1996) 811–820, https://doi.org/10.1002/(SICI)1096-9918(199611)24:12<811::AID-SIA191>3.0.CO;2-Z.
[24] N. Nijem, H. Bluhm, M.L. Ng, M. Kunz, S.R. Leone, M.K. Gilles, Cu^{1+} in HKUST-1: selective gas adsorption in the presence of water, Chem. Commun. 50 (2014) 10144–10147, https://doi.org/10.1039/C4CC02327G.
[25] H.K. Arslan, O. Shekhah, D.C.F. Wieland, M. Paulus, C. Sternemann, M.A. Schroer, S. Tiemeyer, M. Tolan, R.A. Fischer, C. Woll, Intercalation in layered metal–organic frameworks: reversible inclusion of an extended π-system, J. Am. Chem. Soc. 133 (2011) 8158–8161, https://doi.org/10.1021/ja2037996.
[26] O. Shekhah, H. Wang, D. Zacher, R.A. Fischer, C. Woll, Growth mechanism of metal-organic frameworks: insights into the nucleation by employing a step-by-step route, Angew. Chemie Int. Ed. 48 (2009) 5038–5041, https://doi.org/10.1002/anie.200900378.
[27] K. Müller, J. Singh Malhi, J. Wohlgemuth, R.A. Fischer, C. Woll, H. Gliemann, L. Heinke, Water as a modulator in the synthesis of surface-mounted metal–organic framework films of type HKUST-1, Dalton Trans. 47 (2018) 16474–16479, https://doi.org/10.1039/C8DT03310B.
[28] Z.-G. Gu, A. Pfriem, S. Hamsch, H. Breitwieser, J. Wohlgemuth, L. Heinke, H. Gliemann, C. Woll, Transparent films of metal-organic frameworks for optical applications, Microporous Mesoporous Mater. 211 (2015) 82–87, https://doi.org/10.1016/J.MICROMESO.2015.02.048.
[29] P.M. Dietrich, S. Bahr, T. Yamamoto, M. Meyer, A. Thissen, Chemical surface analysis on materials and devices under functional conditions – environmental photoelectron spectroscopy as non-destructive tool for routine characterization,

J. Electron Spectros. Relat. Phenomena 231 (2019) 118–126, https://doi.org/10.1016/J.ELSPEC.2017.12.007.
[30] ISO 18115-1, Surface Chemical Analysis — Vocabulary — Part 1: General Terms and Terms Used in Spectroscopy, Geneva, Switzerland, 2013, 2013.
[31] L. Edwards, P. Mack, D.J. Morgan, Recent advances in dual mode charge compensation for XPS analysis, Surf. Interface Anal. 51 (2019) 925–933, https://doi.org/10.1002/sia.6680.
[32] M.C. Biesinger, Advanced analysis of copper X-ray photoelectron spectra, Surf. Interface Anal. 49 (2017) 1325–1334, https://doi.org/10.1002/sia.6239.
[33] T.H. Fleisch, G.W. Zajac, J.O. Schreiner, G.J. Mains, An XPS study of the UV photoreduction of transition and noble metal oxides, Appl. Surf. Sci. 26 (1986) 488–497, https://doi.org/10.1016/0169-4332(86)90120-0.
[34] V. Di Castro, G. Piredda, Photoinduced reduction of silica supported CuO during XPS irradiation, Chem. Phys. Lett. 114 (1985) 109–113, https://doi.org/10.1016/0009-2614(85)85065-X.
[35] R. Hesse, UNIFIT 2018, UNIFIT Sci. Softw. GmbH. (n.d.). http://home.uni-leipzig.de/unifit/index.html (Accessed October 14, 2019).
[36] ISO 19318:2004, Surface Chemical Analysis - X-Ray Photoelectron Spectroscopy - Reporting of Methods Used for Charge Control and Charge Correction, International Organization for Standardization, Geneva, Switzerland, 2004.
[37] L. Trotochaud, A.R. Head, S. Pletincx, O. Karslıoğlu, Y. Yu, A. Waldner, L. Kyhl, T. Hauffman, H. Terryn, B. Eichhorn, H. Bluhm, Water adsorption and dissociation on polycrystalline copper oxides: effects of environmental contamination and experimental protocol, J. Phys. Chem. B 122 (2018) 1000–1008, https://doi.org/10.1021/acs.jpcb.7b10732.
[38] M.M. Sabri, J. Jung, D.H. Yoon, S. Yoon, Y.J. Tak, H.J. Kim, Hydroxyl radical-assisted decomposition and oxidation in solution-processed indium oxide thin-film transistors, J. Mater. Chem. C 3 (2015) 7499–7505, https://doi.org/10.1039/c5tc01457c.